

HARD X-RAY SPECTROSCOPY AND PULSAR PHASE ANALYSIS OF THE BURSTING X-RAY PULSAR GRO J1744–28 WITH OSSE

M. S. STRICKMAN,^{1,2} C. D. DERMER,¹ J. E. GROVE,¹ W. N. JOHNSON,¹ G. V. JUNG,³ J. D. KURFESS,¹
B. F. PHILIPS,³ G. H. SHARE,¹ S. J. STURNER,^{1,4} D. C. MESSINA,⁵ AND S. M. MATZ⁶

Received 1996 March 19; accepted 1996 April 9

ABSTRACT

We report OSSE observations of the bursting X-ray pulsar GRO J1744–28 made in 1995 December and 1996 January at hard X-ray energies >35 keV. The pulse profile of the persistent (i.e., nonbursting) pulsar emission is fitted with a sinusoid in the energy range 35–90 keV. Residuals reveal a second harmonic amplitude of $3.0\% \pm 0.5\%$ of the fundamental. The distribution of time intervals between bursts measured in January is characterized by a broad flat-topped function with width ≈ 35 minutes and mean ≈ 33 minutes. The burst profile averaged over an ensemble of 104 bursts in the 35–60 keV energy range has FWHM width of 3.6 ± 0.3 s and displays a factor of 2 faster rise time than decay and a pronounced dip in persistent emission after the burst. The phase of the sinusoidal pulse profile during bursts lags the phase prior to bursts by ≈ 90 ms (≈ 1.2 radians), and a 29 ± 6 ms (0.39 ± 0.08 radians) lag persists following the burst. There are no statistically significant spectral differences between the hard X-ray spectra of the bursting and persistent emission in the OSSE energy range, nor is there any evidence of annihilation or neutron capture line emission or cyclotron absorption.

Subject headings: gamma rays: observations — stars: individual (GRO J1744–28) — stars: neutron — X-rays: stars

1. INTRODUCTION

On 1995 December 2, Fishman et al. (1995), using the Burst and Transient Source Experiment (BATSE) on the *Compton Gamma Ray Observatory* (CGRO), discovered an unusual source of intense X-ray bursts in the direction of the Galactic center (see also Kouveliotou et al. 1996b). During the first day of detection, this source, GRO J1744–28, emitted hard X-ray bursts at the rate of ~ 20 hr⁻¹. The rate decreased to ~ 30 day⁻¹ over the next 2 weeks. Following early results from BATSE, the Interplanetary Network, and the Oriented Scintillation Spectrometer Experiment (OSSE) (Hurley et al. 1995; Kurfess et al. 1995), the *Rossi X-ray Timing Explorer* (RXTE) constrained the source to a 21 arcmin² box centered at $l = +0^\circ 02'$, $b = +0^\circ 3'$ (Swank et al. 1996). Further analysis also revealed a positionally coincident bright persistent X-ray source (Paciesas et al. 1996) and X-ray pulsar with a 467 ms period (Finger et al. 1996a) in an 11.8 day binary system (Finger et al. 1996b). The association of the bursting source with the pulsar was established when pulsations were detected in the bursts (Kouveliotou et al. 1996a). This is the first example of a Galactic X-ray binary that is both a pulsar and a burst source.

We report on observations of GRO J1744–28 made with OSSE on CGRO. We perform pulsar timing analysis during the bursting and the nonbursting intervals. We will refer to the emission during nonbursting intervals as the persistent emission. We present the pulse profile of the persistent emission, the interval distribution of bursts, the ensemble-averaged light curve in a 1500 s interval around the burst onsets, the

ensemble-averaged pulsar phase during this same interval, and the spectra for the persistent and bursting emission. We discover a phase lag between the burst and persistent pulsed emission (Jung et al. 1996), which may provide a new diagnostic for mass accretion onto magnetized neutron stars.

2. OBSERVATIONS

The OSSE instrument (Johnson et al. 1993) covers the energy range from ~ 35 keV to 10 MeV. We can isolate pulsar and burst emission by their time signatures, but source confusion due to the relatively large field of view ($3^\circ 8' \times 11^\circ 4'$) means that we cannot extract the persistent unpulsed emission unambiguously, and hence, with the exception of line emission limits, we will not discuss it here.

OSSE observed the region of GRO J1744–28 during 1995 December 14–20 and 1996 January 2–30 with a variety of position angles and instrument configurations. Data were collected at twice-normal gain to optimize the low-energy response. The early Target of Opportunity data from 1995 December and 1996 January 2–12 were used primarily for positioning (Kurfess et al. 1995) and are not used in the analysis described here. Separate localizations of the emissions from the burst source and the pulsar using these data and the data of 1996 January 16–18 produced a 160 arcmin² 95% error box consistent with RXTE. Individual bursts were identified in the data stream with an estimated 99% success rate by manual inspection of counting rates at 2 and 8 s resolution.

3. RESULTS

Data from 1996 January 18–30, during which OSSE was configured for maximum sensitivity, were used to analyze the bursting and persistent pulsar pulse profiles and burst light curves and spectral evolution from a sample of 104 bursts observed with all four OSSE detectors. Studies of the intervals between bursts were performed on a larger set of 260 bursts,

¹ Naval Research Laboratory, Washington, DC 20375-5352.

² strickman@osse.nrl.navy.mil.

³ Universities Space Research Association, Washington, DC 20024.

⁴ NRL/NRC Research Associate.

⁵ SFA, Inc., Largo, MD 20774-5322.

⁶ Northwestern University, Evanston, IL 60208.

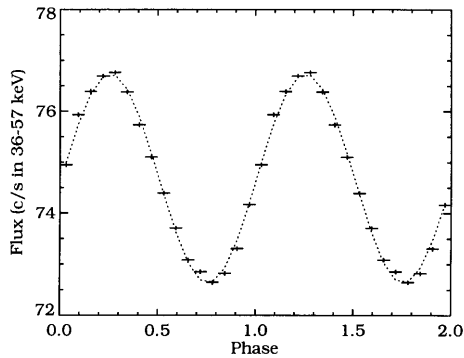


FIG. 1.—Pulse profile of the persistent emission from GRO J1744–28 measured by OSSE during 1996 January 18–30 in the 36–57 keV range. Also shown is the best-fit sinusoid (fundamental only).

which also included those observed with only two detectors. Burst spectra were determined from 219 bursts of this larger sample.

3.1. Pulse Profile for Persistent Emission

We epoch-folded our 32 ms resolution rate data in seven energy bands from 35 to 90 keV, using pulsar and binary ephemerides supplied by BATSE (M. Finger 1996, private communication). The general shape of the resulting pulse profile is sinusoidal (Fig. 1). The best-fit sinusoid gives an unacceptable reduced $\chi^2_\nu = 6.5$ for 13 degrees of freedom. The addition of the second harmonic component with amplitude $3.0\% \pm 0.5\%$ of the fundamental improves the fit to $\chi^2_\nu = 2.3$ for 11 degrees of freedom.

3.2. Interval Distribution of Bursts

We studied the distribution of times between bursts during the period 1996 January 16–30. The observed interval distribution for 260 bursts detected during this period is shown in Figure 2. The minimum observed interval was 10.8 minutes, and the maximum was 466 minutes. The observed interval distribution is the true distribution modulated by OSSE’s visibility window caused by Earth occultation of GRO J1744–28. The two peaks are caused by successive bursts occurring in the same continuous data interval or split between adjacent intervals. The width and rough shape of the true interval distribution can be deduced from the ratio of the number of bursts in each of the peaks.

The form of the true interval distribution was modeled by sampling trial distributions with OSSE’s visibility window and comparing them with the observed interval distribution. Good agreement was found for a distribution of burst separations

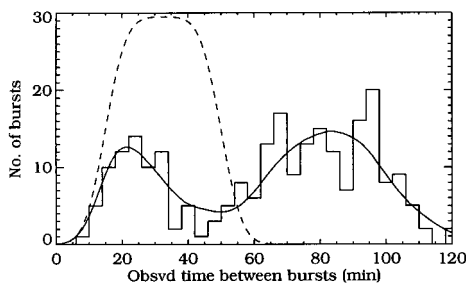


FIG. 2.—Observed interval distribution of times between bursts. The solid curve shows the fitted interval distribution after convolving a model function (dashed curve), described in text, by the visibility window of OSSE.

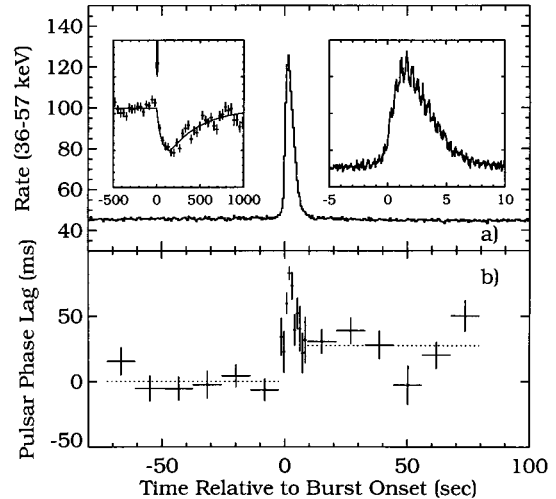


FIG. 3.—Ensemble-averaged light curve in the 36–57 keV band for 104 bursts aligned on (a) the onset of bursts and (b) phase of fitted sinusoid. Upper right inset is detail of burst, clearly showing 2.1 Hz pulsations; upper left inset indicates longer term behavior with postburst dip. The arrow indicates the burst time.

consisting of a flat-topped function with mean ≈ 33 minutes and full width at zero intensity ≈ 35 minutes convolved with a 5 minute rms Gaussian (see Fig. 2). Other smooth, broad functions also yield acceptable agreement. Based on trials with a variety of distributions, we find that the true distribution must be flatter than Gaussian. A simple Gaussian cannot provide the correct number and distribution of short and long intervals.

For the data set 1996 January 18–30, we also searched for correlations between the strength of a burst and the time between bursts for the 56 pairs of bursts in continuous data streams. No correlation was found between burst fluence and the time from the previous burst or the time to the next burst, in agreement with the results of Kouveliotou et al. (1996b). Because the accretion rate may vary, persistent pulsed fluence since the previous burst and until the next burst are better indicators of amount of accreted material than time interval. We compared burst fluence to persistent pulsed fluence and again found no evidence of significant correlation.

3.3. Ensemble-averaged Burst and Pulse Profiles

In order to study the average burst and persistent emission light curves, we aligned and summed individual bursts using the following procedure. The 32 ms rate data were visually inspected to identify a nominal burst onset time. The rate data from each of 104 bursts were aligned on these onset times and were adjusted forward by up to one pulsar period so that pulsar cycles defined by the mean ephemeris would align in phase from burst to burst. The rates were then averaged to produce the 36–57 keV mean burst profile shown in the upper panel of Figure 3. The bursting portion of the ensemble-averaged light curve can be represented by a Gaussian rise and fall with 1.2 ± 0.2 s half-width at half-maximum (HWHM) rise and 2.4 ± 0.2 s HWHM fall times. Pulsations can be observed clearly during the burst (see right-hand inset to Fig. 3). Although Kouveliotou et al. (1996b) do not indicate how their burst durations are defined, the mean of their distribution of durations (~ 20 s) is clearly wider than our mean width. This

may be due to variations in burst duration with time, since these samples are not contemporaneous.

In order to examine longer timescale variations before and after bursts, we have used standard OSSE background-subtraction techniques to produce count rates before and after the bursts. Since we are looking for time signatures locked to burst occurrence times, source confusion can be ignored as it will produce at most a constant systematic offset of the rate. The burst onset time-aligned average over the ensemble of bursts is shown in the left-hand inset in Figure 3, with the burst itself suppressed in order to show detail. In the 36–57 keV energy band displayed, we see clear evidence of a postburst dip with leading and trailing profiles described by exponentials. The e -folding times for the leading and trailing edges are 50 ± 20 s and 370 ± 60 s, respectively, with the dip minimum at 150 ± 50 s after burst onset.

3.4. Pulsar Phase Analysis

We analyzed our data to look for variations in the pulse profile at different times relative to burst onset. Starting with the ensemble-averaged burst profile, we removed the rising and falling trends of the burst by subtracting a burst profile smoothed with a running average one pulsar period wide. The result was a sequence of pulses (each averaged over the 104 burst ensemble) with the general burst trends removed, which allowed us to examine the properties of the pulse profile without the systematics caused by the rise and fall of the bursts. We fitted a sinusoidal model to each pulse, producing a time history of pulse properties. We found that whereas the pulse profile was described by a sinusoid at all times, the phase varied across the burst, as we reported earlier (Jung et al. 1996).

The lower panel of Figure 3 displays the phase of the fitted sinusoids as a function of time from burst onset. The pulsar phase during and after the burst substantially lags the phase prior to the burst. The maximum phase lag of ≈ 90 ms (≈ 0.2 pulsar revolutions; ≈ 1.2 radians) occurs near the peak of the burst. The phase lag then relaxes to a value of 29 ± 6 ms (0.39 ± 0.08 radians) during the interval 10–80 s after burst onset. Stark et al. (1996a, 1996b) have confirmed this with *RXTE* observations. They also note that the phase relaxes back to the preburst value with 500 s e -folding time. Our phases are consistent with this decay out to at least 600 s postburst.

3.5. Spectra of Bursting and Persistent Emission

In order to examine the total burst spectrum, we have subtracted from each burst an estimate of the background and persistent emission obtained just before and after the burst interval and have then averaged the resulting burst spectra for a sample of 219 bursts. The results (Fig. 4) have been fitted from 40 to 150 keV using the standard OSSE forward-folding technique with a model photon number spectrum consisting of a power law times an exponential cutoff: $E^{-\Gamma} e^{-E/E_{\text{fold}}}$ (“PLEXP” model). This procedure yields a power-law index $\Gamma = 2.0 \pm 0.6$ and $E_{\text{fold}} = 15 \pm 3$ keV, with $\chi^2_{\nu} = 1.2$ for 15 degrees of freedom. These values are consistent with those quoted by Swank et al. (1996) at lower energies from observations by *RXTE*. We also fitted simple exponential and blackbody models, but these do not represent the data as well.

We searched for evidence of spectral evolution during bursts on timescales from 32 ms upward. Hardness ratios computed on various intervals are consistent with approxi-

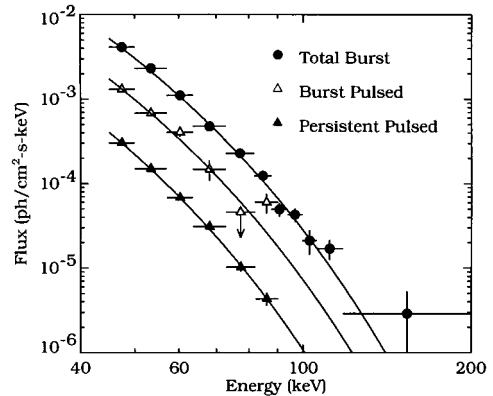


FIG. 4.—Spectra of burst and persistent emission. The total burst spectrum consists of all emission in excess of the average of the pre- and postburst levels. The persistent pulsed spectrum contains all times during which no burst emission is present. Note that the time intervals used for determining the total burst emission are not the same as those for the pulsed burst, so that these two spectra should not be used to determine pulsed fractions.

mately constant folding energy throughout the bursts. In particular, comparing the spectral hardness (50–80 keV/35–50 keV) during the 1.5 s surrounding the burst peak to that during the 2 s surrounding the half-peak intensity in the decay shows a softening of only $-6\% \pm 3\%$, which corresponds to a folding energy change from the best-fit PLEXP model spectrum of approximately -0.6 ± 0.3 keV.

We searched for narrow-line emission at 0.511 and 2.223 MeV in both the total burst and the total persistent spectra. After accounting for the contribution of the diffuse Galactic emission to the total persistent spectrum, we can place a 95% upper limit of 1.5×10^{-4} photons $\text{cm}^{-2} \text{s}^{-1}$ on narrow line emission at 0.511 or 2.223 MeV. The 95% limit on narrow lines in the total burst spectrum is 4×10^{-4} photons $\text{cm}^{-2} \text{s}^{-1}$ for 0.511 or 2.223 MeV emission. There is no evidence for cyclotron absorption features in the total burst spectrum anywhere in the OSSE band. The 95% confidence upper limit on the optical depth of a cyclotron line with 20% HWHM (typical of X-ray pulsars; see Mihara 1995 for line model and typical widths) is 0.25. The depth of narrower lines is more strongly constrained.

We have also examined the persistent and burst pulsar spectra by epoch-folding the 32 ms data over several broad time intervals relative to the starting times of the 104 burst ensemble. Intervals include persistent times (i.e., all times outside of burst), preburst times 30–90 s prior to burst onset, burst times 0–8 s after burst onset, and postburst times 2–6 minutes after burst onset. Fitting the PLEXP model in the 45–90 keV range, we find that the pulsed spectra in the various intervals are consistent in shape with the total burst spectrum, as shown in Figure 4. We find no evidence for dependence of spectral shape on pulsar phase.

4. DISCUSSION

GRO J1744–28 is thought to be a magnetized neutron star powered by Roche-lobe overflow from an evolved subgiant or giant companion, with the system viewed nearly face-on (Daumerie et al. 1996; Sturmer & Dermer 1996). By comparing spin-up rates with luminosity, Daumerie et al. infer a magnetic field of about 10^{12} G, whereas Sturmer & Dermer argue that the spin-up rate and observed quasi-periodic oscillation frequency (Zhang et al. 1996) imply a polar magnetic field

strength $\approx 10^{11}$ G, assuming the validity of the beat-frequency model of Alpar & Shaham (1985). Fields of $4\text{--}10 \times 10^{12}$ G could produce cyclotron lines in the OSSE energy range; none are observed.

The pulse profile is well fitted by a sinusoid with only a weak second-harmonic component. This distinguishes GRO J1744–28 from most accreting X-ray pulsars (for example, see the energy-dependent pulse profiles shown by Mihara 1995). The weakness of the second harmonic indicates that one pole contributes most of the observed emission.

Recent studies (Lewin et al. 1996; Kouveliotou et al. 1996b) suggest that the bursts from GRO J1744–28 come from accretion instabilities rather than from thermonuclear detonation. Spectral softening, typical of type I thermonuclear X-ray bursts (Lewin, van Paradijs, & Taam 1993), is not observed here. The high effective temperature of the bursts and persistent emission from GRO J1744–28 is comparable to that measured for accreting X-ray pulsars rather than type I X-ray bursts. The effective temperature measured in the bursts is too high to sustain a dense surface layer needed for continuous thermonuclear detonation unless the field is $\gtrsim 10^{13}$ G as argued by Lamb, Miller, & Taam (1996). The burst light curve observed from GRO J1744–28 has interesting similarities with the type II bursts of the Rapid Burster, which are thought to result from accretion instabilities. Kouveliotou et al. (1996b) and Lewin et al. (1996) note that the correlation

between burst fluence and time interval to next burst seen in the Rapid Burster is not observed here. Confirming this, we observe no correlation between burst fluence and persistent fluence during the interval to the next burst. Hence, the relaxation oscillator model (see, e.g., Spruit & Taam 1993) for the Rapid Burster does not directly apply.

Our discovery of phase lags between the bursting and persistent pulsed emissions of GRO J1744–28 (Jung et al. 1996) may provide a new diagnostic of mass accretion onto neutron stars. Reservoirs of accreting matter for the bursting and persistent emission may be physically separate and thus accrete along different field lines. Anisotropies in the X-ray emission at different mass accretion rates could also produce phase shifts (see Wang & Welter 1981). Another possibility is that mass accretion events or glitching phenomena could produce phase lags by sudden changes in the moment of inertia of the neutron star, but this is probably ruled out if account is taken of the large amplitude of the phase lag and the relaxation of the pulse profile phase to its preburst value.

We would like to acknowledge Mark Finger of the *CGRO* Science Support Center for supplying BATSE ephemerides as soon as they were available. This work was partially supported by NASA contract DPR S-10987C and the *Compton Gamma Ray Observatory* Guest Investigator Program GRO-95-135.

REFERENCES

- Alpar, M. A., & Shaham, J. 1985, *Nature*, 316, 239
 Daumerie, P., Kalogera, V., Lamb, F. K., & Psaltis, D. 1996, *Nature*, submitted
 Finger, M. H., Wilson, R. B., Harmon, B. A., Hagedorn, K., & Prince, T. A. 1996a, *IAU Circ.* 6285
 Finger, M. H., Wilson, R. B., & van Paradijs, J. 1996b, *IAU Circ.* 6286
 Fishman, G. J., et al. 1995, *IAU Circ.* 6272
 Hurley, K., et al. 1995, *IAU Circ.* 6275
 Johnson, W. N., et al. 1993, *ApJS*, 86, 693
 Jung, G. V., et al. 1996, *IAU Circ.* 6321
 Kouveliotou, C., Kommers, J., Lewin, W. H. G., van Paradijs, J., Fishman, G. J., & Briggs, M. S. 1996a, *IAU Circ.* 6286
 Kouveliotou, C., van Paradijs, J., Fishman, G. J., Briggs, M. S., Kommers, J., Harmon, B. A., Meegan, C. A., & Lewin, W. H. G. 1996b, *Nature*, 379, 799
 Kurfess, J. D., Grove, J. E., Messina, D., & Tueller, J. 1995, *IAU Circ.* 6276
 Lamb, D. Q., Miller, M. C., & Taam, R. E. 1996, *ApJ*, submitted
 Lewin, W. H. G., Rutledge, R. E., Kommers, J. M., van Paradijs, J., & Kouveliotou, C. 1996, *ApJ*, 462, L39
 Lewin, W. H. G., van Paradijs, J., & Taam, R. E. 1993, *Space Sci. Rev.*, 62, 223
 Mihara, T. 1995, Ph.D. thesis, Univ. of Tokyo
 Paciesas, W., et al. 1996, *IAU Circ.* 6284
 Spruit, H. C., & Taam, R. E. 1993, *ApJ*, 402, 593
 Stark, M. J., Baykal, A., Strohmayer, T., & Swank, J. H. 1996a, *IAU Circ.* 6324
 ———. 1996b, *IAU Circ.* 6334
 Sturmer, S. J., & Dermer, C. D. 1996, *ApJ*, submitted
 Swank, J., et al. 1996, *IAU Circ.* 6291
 Wang, Y.-M., & Welter, G. L. 1981, *A&A*, 102, 97
 Zhang, W., Morgan, E., Swank, J., Jahoda, K., Jernigan, G., & Klein, R. 1996, *IAU Circ.* 6300